105 (2026) 107004

Contents lists available at ScienceDirect

Poultry Science

journal homepage: www.elsevier.com/locate/psj

Full-Length Article

Single-cell RNA sequencing reveals depot-specific characteristics of adipose progenitor cells in ducks

Zhixiu Wang [a,1], Chunyan Yang [a,1], Suli Liu [a], Yong Jiang [a], Hao Bai [a], Guobin Chang [a], Guohong Chen [a], Liang Zhao [b,*]

[a] Key Laboratory for Animal Genetics & Molecular Breeding of Jiangsu Province, College of Animal Science and Technology, Yangzhou University, Yangzhou 225009, China

[b] College of Animal Science and Technology, Nanjing Agricultural University, Nanjing 210095, China

ARTICLE INFO

Scientific section: Genetics and Molecular Biology

Key words:
Meat ducks, Single-cell RNA sequencing, Adipose progenitor cells
Differential deposition
Adipogenic properties

ABSTRACT

Depot-specific fat deposition influences carcass yield and meat quality in ducks. To explore regulatory mechanisms, we profiled adipogenic progenitor cells (APCs) from pectoral muscle (PM), subcutaneous (SAT), and visceral adipose tissue (VAT) using single-cell RNA sequencing. Nine major cell types were identified, with APCs being most abundant in VAT and least abundant in PM, consistent with histological findings. Transcriptomic comparisons revealed depot-specific microenvironments: PM was enriched with myogenic-related pathways, SAT with immune and inflammatory responses, and VAT with pro-adipogenic signaling. Next, APCs were regrouped into 5 subclusters. Cluster 0 (PI16^{high} PDGFRB^{high}) enriched in SAT/VAT showed activated signaling of BMP and glycolysis, indicating strong adipogenic potential. Cluster 1 (PDGFRA^{high} F3^{high}) enriched in PM was associated with Wnt signaling, which maintains APCs in a progenitor state. Cell cycle, RNA velocity, and pseudotime analyses indicated that APCs of SAT/VAT were more advanced in differentiation, while APCs of PM retained stronger proliferative capacity. Cell-cell communication analysis further revealed more active paracrine regulation within SAT/VAT, while APCs from PM showed limited signaling interactions. Key depot-specific regulators were identified, including *NEGR1* (PM), *CD36* (SAT), and *RSPO2* (VAT), which may contribute to regulations of the adipogenic process. This study provides the first single-cell atlas of duck APCs across depots, revealing molecular heterogeneity, lineage dynamics, and niche-specific regulation. These findings advance understanding of depot-specific adipogenesis and offer targets to enhance IMF while limiting excessive SAT and VAT, thereby improving both meat quality and production efficiency.

Introduction

Meat ducks are characterized by a short feeding cycle, rapid growth rate, high meat yield, and superior meat quality, holding significant importance in the poultry industry (Yang et al., 2022). In recent decades, the intensive selection for enhanced meat yield and growth rates has substantially improved production efficiency. However, this has also led to excessive deposition of subcutaneous (SAT) and visceral (VAT) adipose tissue, accompanied by reduced deposition of fat in the pectoral muscle (PM). Increasing the content of intramuscular fat is known to improve the tenderness, juiciness, flavor, and overall sensory attributes of duck meat, and is therefore considered a critical indicator of meat quality (Li et al., 2020a; Malgwi et al., 2022). In contrast, excessive deposition of SAT and VAT reduces feed conversion efficiency, compromises carcass quality, and leads to feed waste, ultimately hindering the sustainable development of the duck industry (Cui et al., 2022; Li et al., 2020b; Zhang et al., 2018). Consequently, precise regulation of depot-specific fat deposition has become a central objective in the genetic improvement of meat ducks.

Adipogenic progenitor cells (APCs), with the potential to differentiate into mature adipocytes (Suchanecka et al., 2025), play a fundamental role in the development, expansion, and regeneration of fat tissues (Berry et al., 2014). The total amount and deposition rate of adipose tissue in specific depots are largely determined by the number,

* Corresponding author at: Laboratory of Animal Genetics and Breeding and Molecular Design of Jiangsu Province, College of Animal Science and Technology, No. 567, Wenchang Middle Road, Ganquan Street, Yangzhou City, Jiangsu 225009, PR China.
E-mail address: liang.zhao@njau.edu.cn (L. Zhao).
[1] These authors contributed equally to this work.

https://doi.org/10.1016/j.psj.2026.107004
Received 19 January 2026; Accepted 22 April 2026
Available online 23 April 2026

self-renewal capacity, and differentiation potential of APCs. During embryonic development, APCs from different adipose depots originate from distinct mesenchymal stem cells (Chau et al., 2014; Sebo and Rodeheffer, 2019). Moreover, depot-specific microenvironments contribute to differences in their adipogenic potential and differentiation efficiency. For instance, APCs within the muscle tissue are exposed to various myokines such as myonectin (Sun et al., 2023), irisin (Roca-Rivada et al., 2013), and interleukin −15 (IL-15) (Kang et al., 2018), which have been shown to have important regulatory functions on adipogenesis. As a result, substantial variations exist in the adipogenic capacity and fat deposition rates among different depots.

Current research on fat deposition focuses on individual adipose depots, with limited insights into the comparative regulatory mechanisms underlying depot-specific fat deposition. To address this gap, this study utilized the high-resolution techniques of single-cell RNA sequencing (scRNA-seq) to systematically analyze the cellular landscapes of APCs and their differential regulatory mechanisms of adipogenesis within depots of the SAT, VAT, and PM of a most widely farmed breed in China, the Cherry Valley ducks. We successfully identified key regulatory genes and signaling pathways that might contribute to the differential adipogenic potentials of APCs from the above three depots. This work provides novel mechanistic insights and potential molecular targets for improving meat quality and enhancing the economic efficiency of meat duck production.

Materials and methods

Ethics Statement

All experimental procedures were approved by the China Council on Animal Care and Ministry of Science and Technology of the People's Republic of China. All experimental ducks were managed and handled according to the guidelines established and approved by the Animal Care and Use Committee of the Yangzhou University (No. SYDW-2019015).

Animals and experimen design

The ducks used in this study were purchased from Shuyang Zhongke Seed Poultry Co., Ltd. (Jiangsu, China). One-day-old male Cherry Valley ducks with similar body weights were selected and raised under standardized husbandry conditions, with ad libitum access to feed and water throughout the experimental period. On day 8, the ducks were slaughtered, and samples of pectoral muscle, subcutaneous fat tissue, and visceral fat tissue were promptly collected, with three biological replicates for each tissue type. One portion of each sample was fixed in 4% paraformaldehyde for hematoxylin and eosin (H&E) staining. The remaining two portions were used for preparing single-cell suspensions and for RNA extraction followed by quantitative real-time PCR (RT-qPCR) to validate the expression levels of target genes.

Cell suspension preparation

Subcutaneous fat tissue, visceral fat tissue, and pectoral muscle specimens were sequentially washed with cold PBS (Procell, PB180327, Wuhan, China) and mechanically dissected into 2-4 mm^3 fragments. Tissue dissociation was performed using the Multi-Tissue Dissociation Kit 2 (Miltenyi Biotec, 130-110-203, Bergisch Gladbach, Germany) according to the manufacturer's instructions. The resulting cell suspensions were filtered through a 70 μm cell strainer, followed by centrifugation to obtain the cell sediment. Erythrocytes were lysed by resuspending the precipitate in Red Blood Cell Lysis Buffer (Solarbio, R1011 China). After lysis, the cells were washed, centrifuged, and resuspended. Cell number and viability were assessed using the Countstar® Rigel S2 Fluorescence Cell Analyzer in combination with AO/PI staining reagents (Countstar, RE010212, China). Cells with viability greater than 90% were washed, resuspended, and adjusted to a final concentration of 700–1200 cells/μL for subsequent single-cell library preparation using the 10x Genomics platform.

Single cell library construction and sequencing

Single-cell libraries were constructed using the Chromium Single Cell 3′ Reagent Kits v3 (10x Genomics) following the manufacturer's instructions. Briefly, cell suspensions were loaded onto 10x Chromium controllers for cell lysis, barcode reverse transcription, cDNA amplification, shearing and adapter/index ligation. The PCR product was evaluated using the High Sensitivity DNA assays (PerkinElmer), which showed a fragment size of approximately 1200-1500 bp, indicating that high quality cDNA was synthesised. Final libraries were normalized to 10 nM and sequenced on a NovaSeq 6000 (Illumina).

Data quality control

FastQC was used to assess the quality of raw sequencing data generated by the Illumina platform in FASTQ format. To ensure high-quality data for downstream analyses, raw reads were pre-processed using Trimmomatic, which included trimming low-quality bases with a 4-base sliding window when the average quality dropped below 10, removing low-quality trailing bases, and eliminating adapter sequences through both alignment-based and overlap-based methods. Additionally, reads shorter than 26 bases and those lacking paired-end counterparts were discarded. The resulting high-quality reads, referred to as clean reads, were then re-evaluated using FastQC to confirm their quality before subsequent analyses.

Primary analysis of raw read data

Raw reads were demultiplexed and aligned to the reference genome of anas platyrhynchos (NCBI_ZJU1.0) using the 10x Genomics Cell Ranger pipeline with default parameters. Unique molecular identifiers (UMIs) were counted per gene and per cell barcode to generate digital expression matrices. The cellranger count function handled alignment, barcode and UMI counting, and generated feature-barcode matrices; data from multiple GEM wells were combined and normalized using cellranger aggr (v7.2.0). Secondary quality control was performed in the R package of Seurat (v5.2.0) (Hao et al., 2024), retaining genes expressed in at least three cells and cells expressing at least 500 genes, while removing potential doublets or contaminant cells. Further downstream analyses, including dimensionality reduction, clustering, and visualization, were conducted following the standard protocol of Seurat based on the filtered expression matrix.

Dimensionality reduction, clustering, and cell type annotation

To reduce dimensionality, highly variable genes were first identified, and principal component analysis (PCA) was performed to capture the major sources of variation. The top principal components were selected based on ElbowPlot and JackStraw methods. For nonlinear dimensionality reduction and visualization, Uniform Manifold Approximation and Projection (UMAP) or t-distributed Stochastic Neighbor Embedding (t-SNE) was applied. Cell clustering was then performed using the graph-based Louvain algorithm implemented in Seurat, which constructs a K-nearest neighbor graph based on the PCA-reduced data. Each cluster was annotated based on the expression of canonical marker genes. Differentially expressed genes (DEGs) for each cluster were identified using the FindAllMarkers function of Seurat, providing further insight into cluster identity and functional heterogeneity.

Pseudotime trajectory analysis

Trajectory analysis was conducted using Monocle 3 (Trapnell et al.,

2014), and cell differentiation trajectory was calculated using the learn graph function. The starting point of differentiation was assigned based on the expression of cell proliferation-related genes and built-in cell cycle-related marker genes.

Cell cycle analysis

Cell cycle status of single cells was determined using the Seurat package (v5.2.0). Canonical cell cycle marker genes associated with the S and G2/M phases were used to score each cell through the CellCycleScoring function, which assigns cells into G1, S, or G2/M phase according to their expression profiles.

RNA velocity analysis

According to the previous study (La Manno et al., 2018), we use velocyto to estimate the RNA velocity of each cell. The spliced and unspliced reads were calculated with BAM files generated by 10X Genomics Cell Ranger. The resulting RNA velocity vectors were projected onto the Seurat-derived UMAP to visualize lineage progression and infer cell state transitions.

Functional enrichment analysis

The R package of clusterProfiler (version 4.2.2) (Wu et al., 2021) was used to conduct KEGG (Kyoto Encyclopedia of Genes and Genomes) (Kanehisa and Goto, 2000) enrichment analysis of the DEGs and gene set enrichment analysis (GSEA).

Cell - cell communication analysis

To investigate the potential cell-cell communication networks among different cell types, cell-cell communication analysis was performed using the CellChat R package (v2.0.0) (Jin et al., 2025) based on the scRNA-seq data. The input data included the quality-controlled gene expression matrix and corresponding cell type annotations. CellChat leverages ligand-receptor interaction database to identify significantly expressed ligand-receptor pairs across cell clusters and employs a probabilistic model to quantitatively infer the communication strength between interacting cell types. Subsequently, pathway enrichment analysis was conducted to identify dominant signaling pathways, and a cell-cell communication network was constructed to pinpoint key signal senders, receivers, and core pathways.

RNA extraction and real-time quantitative PCR

Total RNA was extracted from cell samples using the Total RNA Extraction Kit (Solarbio, Beijing, China) following the manufacturer's instructions. RNA quality was detected by an Agilent 2100 Bioanalyzer (Agilent Technologies, Palo Alto, CA, USA), with OD260/280 and OD260/230 ratios of approximately 1.9 and 2.1, respectively. RNA integrity was further verified by 1.0% agarose gel electrophoresis. RNA was reverse transcribed into cDNA according to the instructions of HiScript IV All-in-One Ultra RT SuperMix (Vazyme, Nanjing, China). RT-qPCR was performed using Taq Pro Universal SYBR qPCR Master Mix (Vazyme, Nanjing, China), with GAPDH serving as the internal control gene. Primer information is listed in Supplementary Table 1. The expression levels of all genes were measured using the $2^{-\Delta\Delta ct}$ method (Livak and Schmittgen, 2001).

Statistical analysis

For single-cell transcriptomic sequencing, the analysis of differential gene expression was performed based on the non-parametric Wilcoxon rank sum test of the R package Seurat (v5.2.0). For RT-qPCR, a one-way ANOVA followed by Bonferroni correction was conducted. These data are processed by SPSS 26.0 (IBM, USA) and GraphPad Prism software (version 8), and expressed by means±SD. Statistical differences were indicated as $*p < 0.05$ and $**p < 0.01$.

Results

The construction of single-cell transcriptomic atlas of adipogenic progenitor cells from distinct adipose tissue depots of cherry valley ducks

To systematically investigate the regulatory mechanisms of fat deposition variations in distinct depots of meat ducks, this study focused on elucidating their differences in cellular characteristics of APCs, which determine their adipogenic potentials. Tissues and cells were collected from the PM, and the SAT and VAT adipose tissues of the 8-days-old Cherry Valley ducks (Fig. 1**a**). Histological examination revealed that the density of adipocytes in the VAT was markedly higher than that in the SAT, while no visible adipocytes were detected in the PM (Fig. 1**b**). The adipocytes in SAT were much larger than those in VAT.

After quality control, a total of 38,456 cells were retained for clustering analysis. Utilizing the high-resolution techniques of scRNA-seq, nine distinct cell clusters were identified from all three depots (Fig. 1**c**). These clusters were annotated based on expression profiles of canonical marker genes: Adipose progenitor cells (APCs): *PDGFRA, MMP2*; Erythrocytes (Ery): *RHAG, SPTB*; Myogenic cells (Myo): *MYF5, MYL1*; Macrophages (Mac): *CSF1R, C1QB*; Endothelial cells (Endo): *PECAM1, CDH5*; Neuronal cells (Neu): *SNCA, FOXD3*; T cells (T): *CD3E, SCD247*; Smooth muscle cells (SMCs): *ACTA2, TAGLN*; Hematopoietic stem cells (HSCs): *KIT, HDC* (Fig. 1**d**). Comparative analysis of cluster proportions revealed that the cluster of APCs constituted a major cell population in all three depots, with the highest abundance observed in the VAT. In contrast, the population of Mac was more enriched in the SAT and VAT compared to the PM (Fig. 1**e**). In summary, our histological analysis showed clear differences in adipocyte depositions in three depots, and our scRNA-seq analysis successfully identified the population of APCs in all depots, laying the groundwork for further molecular investigations.

Depot-specific microenvironment might contribute to variations in the adipogenic properties of adipose progenitor cells

Transcriptomes of all cells in the PM, SAT, and VAT were compared to show their differences in endogenous microenvironment caused by the depots of deposition (Fig. 2). The results showed that the number of genes that were positively regulated (Fig. 2**a**) in the PM (3275 genes) was much larger than those of the SAT (251 genes) and VAT (455 genes), while the number of genes that were negatively regulated (Fig. 2**b**) between depots was comparable (1513, 1637, and 1512 genes, respectively). The heatmap of differential expressed genes showed clear distinction between three depots, showing large differences in their transcriptomes (Fig. 2**c**).

The top 300 genes of the positively expressed markers in each depot were used for pathway analysis (Fig. 2**d-f**). As shown in Fig. 2d, the enriched terms of GO biological processes in the PM group were mostly correlated with muscle development regulation, including terms of “muscle system process”, “neuromuscular process”, “regulation of ATP-dependent activity”, “calcium ion transmembrane transport”, “ERBB2 signaling pathway”. In contrast, the GO terms enriched in the SAT group were mostly involved in the immune function and inflammation, such as terms of “erythrocyte differentiation”, “T cell co-stimulation”, “lymphocyte co-stimulation” (Fig. 2**e**). The appearance of these enriched pathways might be correlated with the largest adipocyte size identified in the SAT group as shown in Fig. 1b. Notably, the pathways related to active adipogenesis were found in the VAT group including “transforming growth factor beta receptor superfamily signaling pathway”, “response to BMP”, “positive regulation of angiogenesis”, “positive regulation of MAP kinase activity”, and “lipid import into cell”

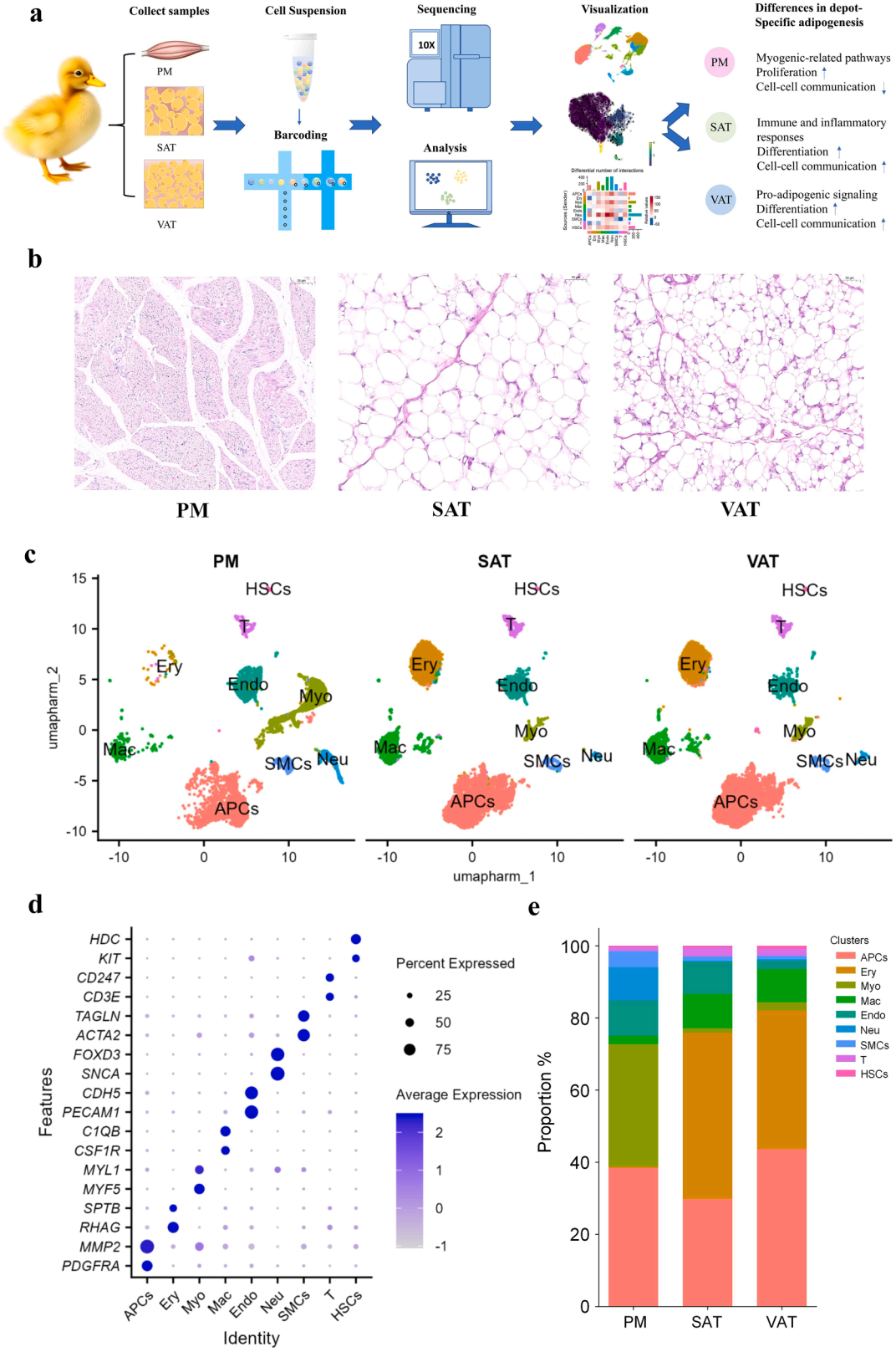

Fig. 1. The single-cell transcriptomic analysis reveals the heterogeneity of cell populations in different adipose depots. (a) Schematic overview of the experimental workflow for investigating regulatory mechanisms of depot-specific fat depositions. (b) Representative H&E staining images of the pectoral muscle (PM), subcutaneous adipose tissue (SAT), and visceral adipose tissue (VAT). (c) UMAP visualization of major cell clusters identified across different adipose depots, including adipogenic progenitor cells (APCs), erythrocytes (Ery), myocytes (Myo), macrophages (Mac), endothelial cells (Endo), neurons (Neu), T cells (T), smooth muscle cells (SMCs), and hematopoietic stem cells (HSCs). (d) Cell-specific markers are shown by violin plot. (e) Proportional distribution of identified cell clusters within each adipose depot.

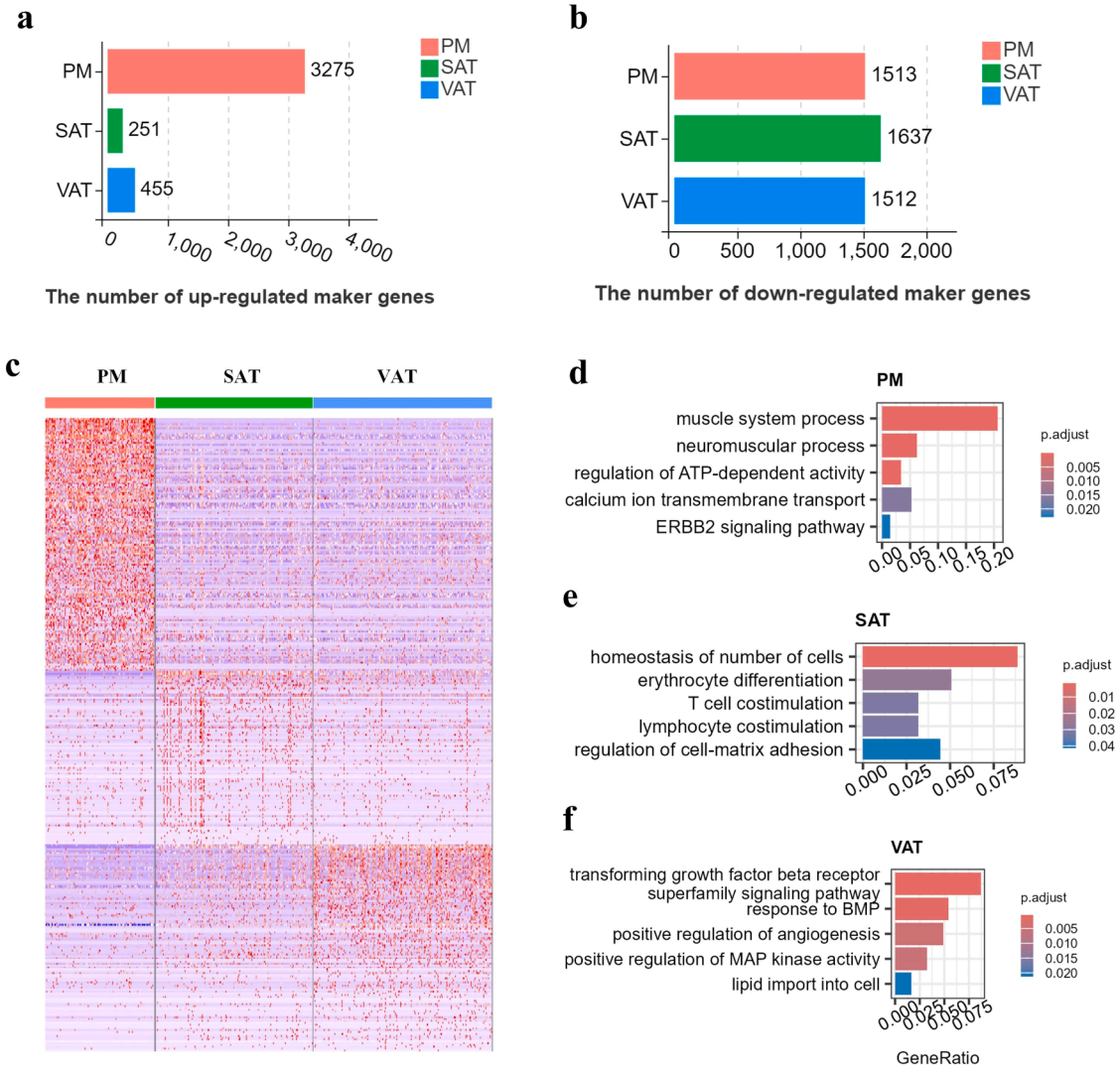

Fig. 2. Comparative analysis of transcriptomes of all cells in PM, SAT, and VAT. (a) Histogram of the number of differentially up-regulated maker genes between the three depots. (b) Histogram of the number of differentially down-regulated maker genes between the three three depots. (c) Heatmap of differentially expressed genes between the three three depots. (d) Enriched Gene Ontology (GO) terms of biological process based on top 300 genes of the positively expressed markers in PM. (e) Enriched Gene Ontology (GO) terms of biological process based on top 300 genes of the positively expressed markers in SAT. (f) Enriched Gene Ontology (GO) terms of biological process based on top 300 genes of the positively expressed markers in VAT.

(Fig. 2**f**). Therefore, the transcriptomes of each adipose depot showed clear distinctions, which constitute distinct microenvironments for the adipogenic regulations of the APCs. In addition, we randomly selected five genes from three depots-specific genes and measured their expression using RT-qPCR (Fig. 2**h**). The results were consistent with the single-cell results, further demonstrating the reliability of single-cell data.

Functional differences of the APCs from different adipose depots

To further explore the potential molecular mechanisms underlying depot-specific fat deposition, we focused on APCs cluster derived from the PM, SAT and VAT (Fig. 3**a**). Comparison of depot-specific gene expression in APCs revealed that APCs from different adipose depots exhibit distinct functional characteristics (Fig. 3**b–d**). Specifically, genes such as *BDNF, NEGR1, DLK1*, and *ALDH1A2* were highly expressed in APCs of the PM (Fig. 3**b**); *CD36, FGF16, BMP5*, and *CCN3* were predominantly expressed in APCs of the SAT (Fig. 3**c**); while *HMGA1, RSPO2, GATA6* and *RUNX1* were significantly upregulated in APCs of the VAT (Fig. 3**d**).

To investigate the biological functions associated with these depot-specific enriched genes, we performed functional enrichment analysis for APCs from each adipose depot (Fig. 3**e-g**). The results showed that PM-derived APCs have both characteristics of "stem cell development" and "fat cell differentiation". Additionally, their adipogenic potential can be affected by various factors including oxidative stress, mechanical stimuli, carbohydrates, glucocorticoids, calcium ions, and nitric oxide, as well as signals from the WNT and ERK pathways (Fig. 3**e**). The APCs in the SAT showed strong potentials for fibrotic differentiation as GO terms of "extracellular matrix organization", "cell-substrate adhesion", "collagen metabolic process", "cell adhesion mediated by integrin", "smooth muscle cell migration", "integrin-mediated signaling pathway", and "response to transforming growth factor beta" were enriched (Fig. 3**f**). In addition, the APCs in the SAT also response to the regulation of retinoic acid and insulin-like growth factor receptor signaling. Similarly, the APCs in the VAT also enriched multiples term related to the fibrotic differentiation of APCs, such as terms of "connective tissue development", "cell-matrix adhesion", "fibroblast proliferation", and "transformation growth factor receptor superfamily signaling pathway" (Fig. 3**g**). In addition, the enrichment of "long-chain fatty acid transport"

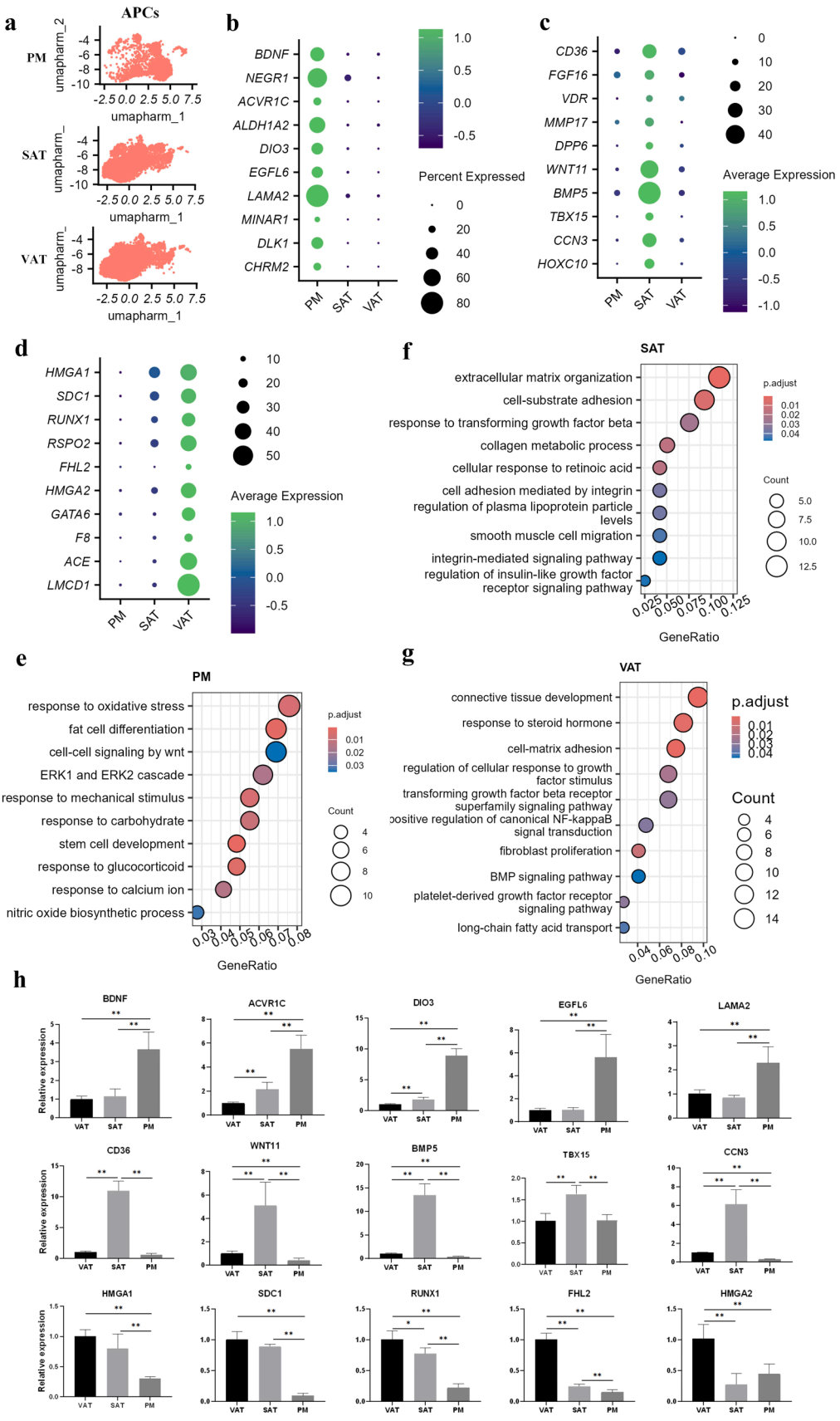

Fig. 3. Transcriptomic analysis of the APCs derived from distinct adipose depots. (a) UMAP plots showing the distribution of the APCs in the PM, SAT, and VAT. (b-d) Signature genes that are differentially upregulated in the APCs from the PM (b), SAT(c), and VAT (d). (e-g) Functional enrichment analysis of differentially upregulated genes (top 150) in APCs from the PM (e), SAT (f), and VAT (g). Note: PM, pectoral muscle; SAT, subcutaneous adipose tissue; VAT, visceral adipose tissue. (h) Measurement of relevant gene expression by RT-qPCR.

and "BMP signaling pathway" showed enhanced adipogenic differentiation potentials of APCs in the VAT. In summary, the APCs in distinct depots of the Cherry Valley ducks showed great differences in their cellular characteristics, signaling transductions and impacts of endogenous factors. The complexity of their transcriptomes, including the presence of fibrotic characteristics, reflects the potential heterogeneity among APCs, warranting further investigation.

In addition, we randomly selected five genes from each adipose depot-specifically expressed region for RT-qPCR validation (Fig. 3**f**). The results were consistent with the single-cell sequencing data, further demonstrating the reliability of the sequencing results.

The subtypes of adipose progenitor cells in distinct depots and their transcriptomic characteristics

To further investigate the molecular regulatory mechanisms of APCs in different adipose depots, we performed subclustering analysis on the APCs. Based on the expression of known marker genes, five subclusters were identified (Fig. 4**a-c**): Cluster 0 ($PI16^{high}$ $PDGFRB^{high}$ APCs), Cluster 1 ($PDGFRA^{high}$ $F3^{high}$ APCs), Cluster 2 ($PDGFRA^{low}$ $F3^{low}$APCs), Cluster 3 ($PDGFRA^{high}$ $CD9^{high}$ APCs), and Cluster 4 ($FMOD^{high}$ APCs). In terms of cellular composition, cells from Clusters 0 and 1 together accounted for over 80% of all APCs (Fig. 4**d**). Notably, the proportion of Cluster 0 was significantly lower in the PM compared to that in the SAT and VAT, whereas Cluster 1 was more abundant in the PM than in the other two depots (Fig. 4**d**).

To further elucidate the different properties of cells from Cluster 0 and Cluster 1, the transcriptomes of Culster 1 was compared with that of the Cluster 0 (Fig. 4**e-h**). Functional enrichment analysis revealed that the BMP signaling pathway was enriched in Cluster 0, while the canonical Wnt signaling pathway was enriched in Cluster 1 (Fig. 4**e-f**). This finding suggests that the differing adipogenic properties of the APCs in the PM and SAT and VAT may be influenced by these two important signaling pathways. The GSEA demonstrated that pathways relate to glycolysis, such as "glucose catabolic process to pyruvate"and "glycolytic process through glucose-6-phosphate"were enhanced in cells of the Cluster 0 compared to those of Cluster 1 (Fig. 4**g**), implying notable differences in energy metabolism between the two clusters. Moreover, genes of *RSPO2, AHRR, THY1, WNT2, ITGB3, CHRDL1, PRRX1, ZNF469*, and *PAMR1* are among the top up-regulated genes in Cluster 0, while genes of *CHRM2, FREM1, DIO3, ALDH1A2, ACVR1C, BDNF, NEGR1, GFRA2*, and *NID1* were mostly expressed in Cluster 1(**Fig. h**). These genes might serve as key regulatory factors for the differential adipogenic properties of APCs in the three adipose depots.

The cellular characteristics and developmental relationships between subtypes of APCs

To better understand the cellular characteristics of the different subtypes of the APCs, we performed a cell cycle analysis using the R package Seurat. The results indicated that Cluster 0 had the lowest ratio of cells in the G2M phase, suggesting a reduced capacity for proliferation (Fig. 5**a-b**). Consistently, we observed a significantly higher number of cells in the G1 and S phases in the SAT and VAT compared to the PM (Fig. 5**c-d**). This suggests that the cells in the SAT and VAT have likely lost their stem cell properties and are more prone to differentiation rather than proliferation.

To further investigate the developmental relationships and dynamic transitions between subtypes of the APCs, RNA velocity and pseudotime trajectory analysis were performed (Fig. 5**e-f**). The arrows in the streamline of RNA velocity analysis (Fig. 5**e**) indicate the directions of cellular state transition between the subpopulations of the APCs. The Results showed that the chances of cells transiting between Cluster 0 and Cluster 1 were low in the PM and VAT, while there is a small portion of cells in Cluster 0 of the SAT tend to develop into cells of the Cluster 1. In addition, the pseudo-trajectory analysis showed that cells of the Cluster 0, 1, and 2 had the same developmental origins in the PM, but no developmental relationships were found for cells of different clusters in the SAT and VAT (Fig. 5**f**). However, noticeably, cells of Cluster 0 were developmentally more advanced than cells of Cluster 1 (Fig. 5**g**). In summary, the cell cycling and developmental relationship analysis found that the APCs in the SAT and VAT showed more tendency to differentiation and more advanced in development than the APCs in the PM, which might explain their differences in adipogenic potentials.

Cell-cell communications in the local microenvironment exhibit differential regulatory functions on the APCs

The adipogenic properties of APCs can be significantly influenced by the local microenvironment. To investigate this, we analyzed the intercellular interactions between APCs and other cell types in the PM, SAT, and VAT using the R package CellChat v2. Our analysis focused on ligand-receptor interactions to identify distinct signaling patterns and variations in communication intensity among different cell types. The results indicated that both the number and strength of cell-cell communications were significantly higher in the SAT and VAT compared to the PM (Fig. 6**a**). Consistently, the numbers of signals received and secreted by the APCs within the PM were considerably lower when compared to those in the SAT (Fig. 6**b**) or VAT (Fig. 6**c**). In addition, the number of intercellular interactions (Fig. 6**a**) and the number of signals secreted by the APCs (Fig. 6**d**) within the VAT were much higher than those within the SAT. The above findings suggest that the APCs in the SAT and VAT are more strongly regulated by signals secreted from nearby cells.

The relative information flow/interaction strength of each signaling pathway was compared to show the altered signaling pathways between three adipose depots (Fig. 6**e**). The results showed that the signaling communications through pathways of SEMA7, CNTN, NEGR, ADGRA, and SELPLG are the top 5 enriched pathways with the PM, while pathways of CYPA, THYE1, HSPG, VTN, and VWF were comparably enriched within the SAT and VAT. We also analyzed the expression of genes involved in these altered signaling pathways (Fig. 6**f**). The gene expression of *PTN, PDGFA, CNTN1*, and *NEGR1* was significantly higher, while the expression of *SLIT3, GDF15, FLRT2*, and *VTN* was significantly lower, in the PM compared to those in the SAT and VAT. Interestingly, NEGR1 was also identified as one of the unique marker genes for the APCs in the PM. Additionally, we measured the expression of *PTN, PDGFA, CNTN1, NEGR1, SLIT3, GDF15, FLRT2*, and *VTN* in the three depots using RT-qPCR (Fig. 6**g**). The results were consistent with the single-cell analysis findings. Therefore, the signals and corresponding signaling pathways identified in this study hold great importance for elucidating the regulatory functions of other types of cells on the APCs.

Discussion

Fat is not only an important form of energy reserve in animal organisms but also plays a crucial role in maintaining metabolic balance, regulating endocrine function, and influencing meat quality. However, different adipose depots have distinct contributions. This study constructed single-cell transcriptome profiles of APCs from three adipose depots (PM, SAT, and VAT) in Cherry Valley ducks. The results revealed distinct differences in morphology, gene expression, signaling pathway activation, and intercellular communication among these depots, which collectively determine their varying adipogenic potential.

The formation and accumulation of adipose tissue are critically dependent on the presence and activity of APCs. Previous studies have shown that the proportion, stemness, and differentiation tendency of APCs in different adipose depots, which may be an important factor causing different deposition capacities of adipose depots (Nahmgoong et al., 2022). In this study, nine distinct cell clusters were identified from PM, SAT, and VAT, among which the cluster of APCs constituted a major cell populations in all three depots, with the highest abundance

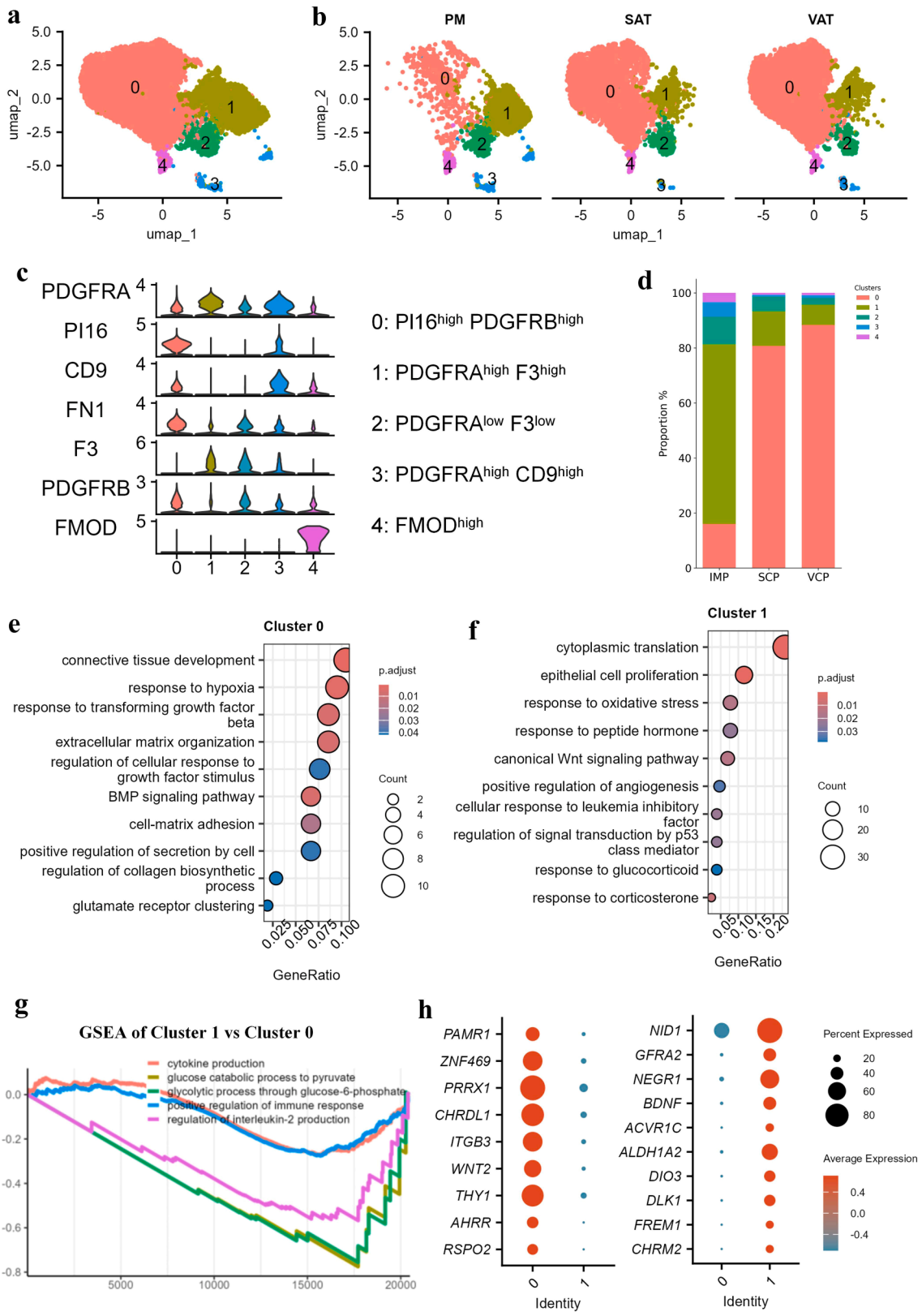

Fig. 4. The compositional differences of APCs from different depots and their cellular characteristics. (a) UMAP visualization of APCs from different depots. (b) Distribution of APC suclusters across different adipose depots. (c) Expression profiles of key marker genes across the five APCs subclusters. (d) Proportional distribution of the five APC subclusters. (e) Enriched Gene Ontology (GO) terms of biological process based on top 150 genes up-regulated in Cluster 0 compared to those in Cluster 1. (f) Enriched GO terms of biological process based on top 150 genes up-regulated in Cluster 1 compared to those in Cluster 0. (g) Enriched terms of Gene Set Enrichment Analysis (GSEA) based on genes compared of Cluster 1 to Cluster 0. (h) Differentially expressed genes between Cluster 0 and Cluster 1.

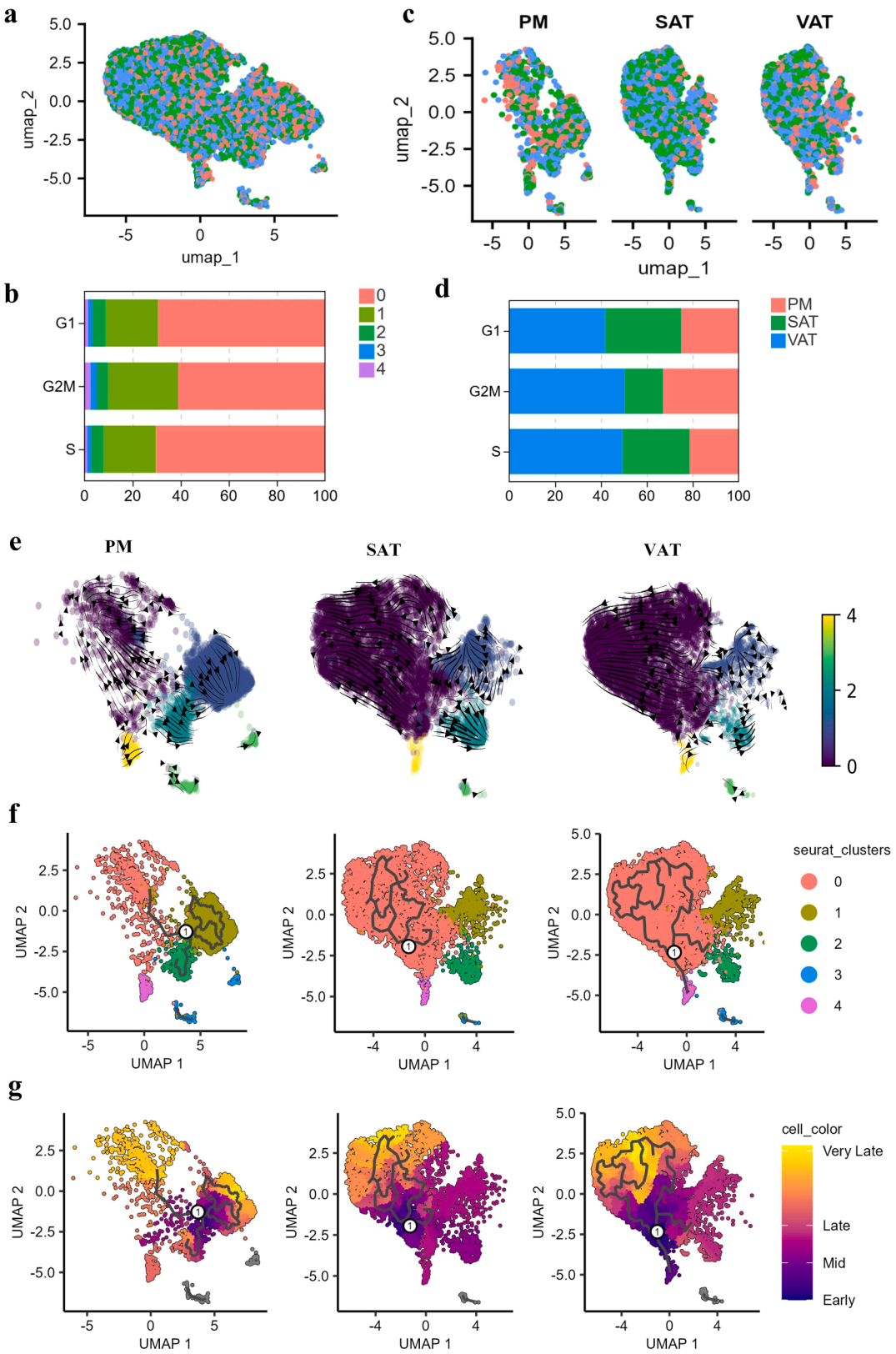

Fig. 5. The cellular characteristics and developmental relationships between subtypes of APCs. (a) Cell cycle analysis of different subtypes of the APCs. (b) The proportion distribution of G1, G2M and S phases in the cell cycle analysis of different subtypes of the APCs. (c) Cell cycle analysis of APCs in the PM, SAT, and VAT. (d) The proportion distribution of G1, G2M and S phases in the cell cycle analysis of APC in three depots. (e) RNA velocity analysis between subtypes of the APCs in PM, SAT, and VAT, respectively. (f) Pseudotime trajectory analysis between subtypes of the APCs in PM, SAT, and VAT, respectively. (g) Heatmap of pseudotime trajectories between subtypes of the APCs in PM, SAT, and VAT, respectively.

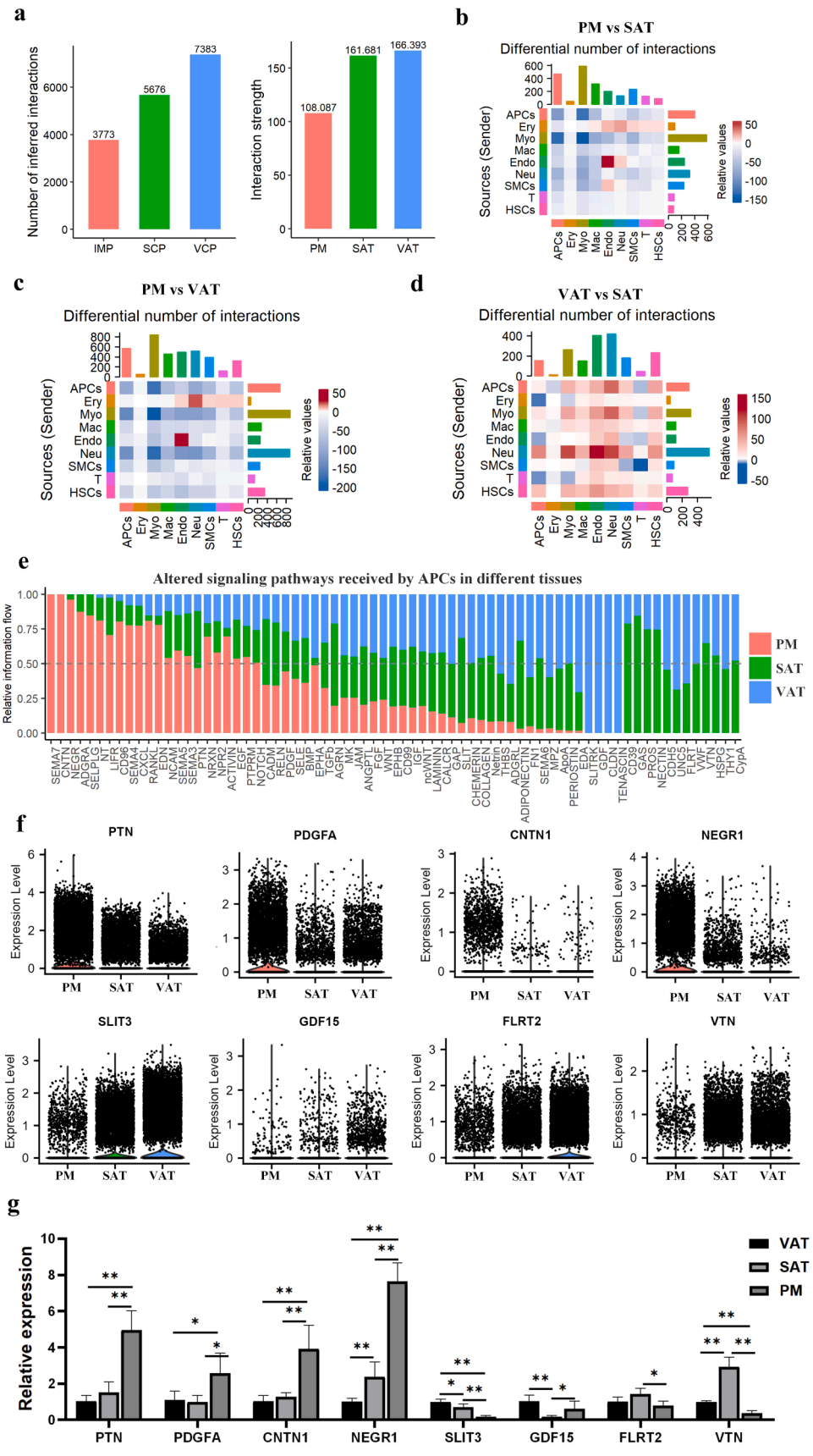

(caption on next page)

Fig. 6. Cell-cell communication networks between different clusters in different adipose depots. (a) Statistical analysis of the number and strength of intercellular communication in three depots. (b) The differential numbers of interactions between cell types within the PM compared to SAT. (c) The differential numbers of interactions between cell types within the PM compared to VAT. (d) The differential numbers of interactions between cell types within the VAT compared to SAT. (e) Comparative analysis of the relative information flow/interaction strength of each signaling pathway among the three adipose depots. (f) Expression of differential genes involved in altered signaling pathways in three adipose depots. (g) Measurement of relevant gene expression by RT-qPCR.

observed in VAT and the least in PM. This trend is consistent with the changes in the density of adipocyte distribution in histological observations. This further confirms that there are significant differences in fat deposition in the three depots, and that APCs play an important role in fat deposition.

Fat deposition is not only determined by the number of APCs, but also regulated by the surrounding microenvironment. Macotela et al. showed that APCs in different mouse fat depots have significant differences in gene expression, differentiation potential, and response to environmental or genetic factors (Macotela et al., 2012). In our study, Transcriptomes of all cells in the three depots revealed depot-specific microenvironments that shape APCs adipogenic potential. In PM, the upregulated genes were were mostly correlated with muscle development regulation, suggesting that this site may be affected by myogenic signals, limiting the adipose differentiation potential of local APCs. SAT was enriched in immune and inflammation-related pathways, such as T cell/lymphocyte co-stimulation, suggesting an immune-mediated niche that promotes adipocyte hypertrophy—consistent with histological observations of larger adipocytes in SAT. VAT, by contrast, showed enrichment in pathways related to adipogenesis and tissue remodeling, including BMP response, positive regulation of angiogenesis, and lipid import into cell, reflecting a microenvironment favorable for adipose expansion. Collectively, these findings highlight depot-specific microenvironmental heterogeneity as a key determinant of regional adipogenesis.

APCs from different adipose depots displayed distinct molecular regulatory mechanisms. Reclustering identified five APC subpopulations with clear functional specializations. Cluster 0 ($PI16^{high}$ $PDGFRB^{high}$), mainly distributed in SAT and VAT, was enriched in the BMP signaling pathway, whereas Cluster 1 ($PDGFRA^{high}$ $F3^{high}$), predominantly found in PM, was enriched in the canonical Wnt pathway. BMP signaling has been well documented to promote adipogenesis (Constant et al., 2025), with BMP2/4 activating SMAD and p38 cascades and inducing PPARγ expression to drive preadipocyte differentiation (Blázquez-Medela et al., 2019; Schreiber et al., 2017). In contrast, The canonical Wnt pathway suppresses PPARγ and C/EBPα expression, thereby blocking terminal differentiation and maintaining progenitors in an undifferentiated state (Li et al., 2023; Xu et al., 2024; Yang Loureiro et al., 2023). Consistent with these pathway activities, GSEA revealed that glycolysis-related pathways were more highly enriched in Cluster 0, indicating a metabolically active, differentiation-prone state, whereas Cluster 1 exhibited features of an undifferentiated progenitor phenotype with conserved energy metabolism.

Depot-specific gene expression further reinforced the functional differences among adipose tissues. In SAT, enrichment of pro-adipogenic factors such as *CD36* and *BMP5* suggested stronger differentiation activity. *CD36*, a key protein involved in fatty acid uptake, is closely associated with adipocyte maturation (Ashaq et al., 2024; Hu et al., 2024; Li et al., 2022). In VAT, genes such as *RUNX*1 and *RSPO2* were highly expressed; notably, *RSPO2* has been shown to induce adipose tissue hypertrophy and insulin resistance in mice(Dong et al., 2022). In contrast, PM was characterized by high expression of *NEGR1, DLK1*, and *EGFL6*, all of which are known inhibitors of adipogenesis or maintain progenitors in an undifferentiated state. *DLK1* is a well-established negative regulator of adipocyte differentiation (Smas and Sul, 1993; Sul, 2009; Zhang et al., 2019), while *NEGR1*, originally studied in the nervous system, has recently been implicated in metabolic regulation. Mouse models have demonstrated that loss of *NEGR1* leads to increased white adipose tissue and insulin resistance, indicating its role in suppressing fat accumulation and promoting energy metabolism (Boender et al., 2014). Similarly, *NEGR1* deficiency was shown to cause ectopic fat deposition (Joo et al., 2019), particularly in adipose and liver tissues, consistent with the restricted adipogenic potential observed in PM. Collectively, these findings highlight the molecular heterogeneity underlying depot-specific adipogenesis.

Cell cycle and RNA velocity and pseudotime trajectory analyses provided dynamic insights into depot-specific differences. APCs in PM were more inclined to maintain stemness and proliferation, whereas those in SAT and VAT predominantly occupied differentiation-related states, suggesting a higher propensity for adipogenesis. This is consistent with previous reports showing that adipose progenitors display distinct proliferative and differentiation capacities depending on their microenvironment (Hepler et al., 2018). RNA velocity and pseudotime trajectory analysis further revealed that PM clusters (0, 1, and 2) shared a common origin with relatively stable lineage relationships, while trajectories in SAT and VAT were more dispersed, likely influenced by local Wnt, BMP, and inflammatory signals (Cristancho and Lazar, 2011; Gesta et al., 2007)[39, 40]. Together, these findings suggest that PM APCs favor self-renewal, whereas SAT and VAT APCs undergo more rapid differentiation, thereby contributing to depot-specific fat deposition-supporting recent perspectives on the heterogeneity of adipose progenitors (Rivera-Gonzalez et al., 2025) .

Cell-cell communication within the microenvironment plays a key role in shaping APC behavior. The recently proposed "Adipocyte Precursor Niche" model points out that endothelial cells, immune cells, smooth muscle cells and fibroblasts can jointly affect the proliferation and directional differentiation of APCs (Kesharwani and Brown, 2024; Altun et al., 2022). Consistently, Pyrina et al. reported that immune cells and endothelial cells significantly affect the fate of APCs through microenvironmental regulation (Pyrina et al., 2020), while APCs themselves can modulate their maintenance and differentiation through PPARγ-mediated VEGF signaling with endothelial cells (Jiang et al., 2017). This study revealed that APCs in the VAT and SAT exhibited a greater number and stronger interactions with other cell types compared to those in the PM, with the VAT showing the most pronounced effect. These findings suggest that APCs in the SAT and VAT are more strongly regulated by paracrine signals from neighboring cells, thereby influencing their proliferative and adipogenic potential. Distinct signaling landscapes were observed across depots, with PM enriched in SEMA7, CNTN, NEGR, ADGRA, and SELPLG pathways, while SAT and VAT favored CYPA, THY1, HSPG, VTN, and VWF pathways. These divergent patterns underscore unique microenvironmental cues shaping APC fate. Gene expression analysis further revealed elevated *PTN, PDGFA, CNTN1*, and *NEGR1* in the PM, contrasting with higher *SLIT3, GDF15, FLRT2*, and *VTN* in SAT/VAT. Notably, *NEGR1* was identified as a PM-specific APC marker, suggesting a role in restraining adipogenesis. Together, these findings highlight depot-dependent signaling programs governing APC regulation.

Conclusion

In summary, this study presents the single-cell transcriptomic atlas of APCs from PM, SAT, and VAT adipose depots in Cherry Valley ducks, uncovering striking depot-specific heterogeneity in cell composition, differentiation potential, and intercellular communication. We identified key regulatory genes and signaling pathways, such as *NEGR1* in intramuscular APCs, *CD36* in subcutaneous APCs, and *RSPO2* in visceral APCs—that govern regional adipogenesis through distinct Wnt- and

BMP-mediated programs. These findings provide novel mechanistic insights into depot-specific fat deposition and highlight potential molecular targets for precisely enhancing intramuscular fat while reducing excessive subcutaneous and visceral fat, thereby offering new strategies to improve both meat quality and production efficiency in ducks.

Declaration of interest

The authors declare that they have no known competing financial interests or personal relationships that could have appeared to influence the work reported in this paper.

Financial support statement

This work was supported by the National Key Research and Development Project of China (2023YFD1300301), National Natural Science Foundation (32472890) and China Agriculture Research System of MOF and MARA (CARS-42-3).

Data availability

The RNA-seq raw data have been submitted to NCBI SRA (SUB15530648).

CRediT authorship contribution statement

Zhixiu Wang: Writing – review & editing, Supervision, Resources, Project administration, Funding acquisition, Data curation, Conceptualization. **Chunyan Yang:** Writing – original draft, Visualization, Validation, Software, Methodology, Investigation, Data curation. **Suli Liu:** Visualization, Validation, Methodology, Data curation. **Yong Jiang:** Validation, Supervision, Investigation. **Hao Bai:** Validation, Supervision, Investigation. **Guobin Chang:** Validation, Resources, Data curation, Conceptualization. **Guohong Chen:** Writing – review & editing, Supervision, Resources, Project administration, Funding acquisition, Data curation, Conceptualization. **Liang Zhao:** Writing – review & editing, Validation, Software, Methodology, Data curation, Conceptualization.

Supplementary materials

Supplementary material associated with this article can be found, in the online version, at doi:10.1016/j.psj.2026.107004.

References

Altun, I., Yan, X., Ussar, S., 2022. Immune cell regulation of white adipose progenitor cell fate. Front. Endocrinol. 13, 859044.
Ashaq, M.S., Zhang, S., Xu, M., Li, Y., Zhao, B., 2024. The regulatory role of CD36 in hematopoiesis beyond fatty acid uptake. Life Sci. 339, 122442.
Berry, R., Jeffery, E., Rodeheffer, M.S., 2014. Weighing in on adipocyte precursors. Cell Metab. 19 (1), 8–20.
Blázquez-Medela, A.M., Jumabay, M., Boström, K.I., 2019. Beyond the bone: bone morphogenetic protein signaling in adipose tissue. Obes. Rev. 20 (5), 648–658.
Boender, A.J., van Gestel, M.A., Garner, K.M., Luijendijk, M.C., Adan, R.A., 2014. The obesity-associated gene Negr1 regulates aspects of energy balance in rat hypothalamic areas. Physiol. Rep. 2 (7), e12083.
Chau, Y.Y., Bandiera, R., Serrels, A., Martínez-Estrada, O.M., Qing, W., Lee, M., Slight, J., Thornburn, A., Berry, R., McHaffie, S., Stimson, R.H., Walker, B.R., Chapuli, R.M., Schedl, A., Hastie, N., 2014. Visceral and subcutaneous fat have different origins and evidence supports a mesothelial source. Nat. Cell Biol. 16 (4), 367–375.
Constant, B., Kamzolas, I., Yang, X., Guo, J., Rodriguez-Fdez, S., Mali, I., Rodriguez-Cuenca, S., Petsalaki, E., Vidal-Puig, A., Li, W., 2025. Distinct signalling dynamics of BMP4 and BMP9 in brown versus white adipocytes. Sci. Rep. 15 (1), 15971.
Cristancho, A.G., Lazar, M.A., 2011. Forming functional fat: a growing understanding of adipocyte differentiation. Nat. Rev. Mol. Cell Biol. 12 (11), 722–734.
Cui, X., Gou, Z., Jiang, Z., Li, L., Lin, X., Fan, Q., Wang, Y., Jiang, S., 2022. Dietary fiber modulates abdominal fat deposition associated with cecal microbiota and metabolites in yellow chickens. Poult. Sci. 101 (4), 101721.
Dong, H., Sun, W., Shen, Y., Baláz, M., Balázová, L., Ding, L., Löffler, M., Hamilton, B., Klöting, N., Blüher, M., Neubauer, H., Klein, H., Wolfrum, C., 2022. Identification of a regulatory pathway inhibiting adipogenesis via RSPO2. Nat. Metab. 4 (1), 90–105.
Gesta, S., Tseng, Y.H., Kahn, C.R., 2007. Developmental origin of fat: tracking obesity to its source. Cell 131 (2), 242–256.
Hao, Y., Stuart, T., Kowalski, M.H., Choudhary, S., Hoffman, P., Hartman, A., Srivastava, A., Molla, G., Madad, S., Fernandez-Granda, C., Satija, R., 2024. Dictionary learning for integrative, multimodal and scalable single-cell analysis. Nat. Biotechnol. 42 (2), 293–304.
Hepler, C., Shan, B., Zhang, Q., Henry, G.H., Shao, M., Vishvanath, L., Ghaben, A.L., Mobley, A.B., Strand, D., Hon, G.C., Gupta, R.K., 2018. Identification of functionally distinct fibro-inflammatory and adipogenic stromal subpopulations in visceral adipose tissue of adult mice. Elife 7, e39636.
Hu, Y.X., Liang, Q., Li, A., 2024. Mechanism of fatty acid transposase (CD36) promoting fat accumulation in mule ducks. Poult. Sci. 103 (12), 104268.
Jiang, Y., Berry, D.C., Jo, A., Tang, W., Arpke, R.W., Kyba, M., Graff, J.M., 2017. A Ppargamma transcriptional cascade directs adipose progenitor cell-niche interaction and niche expansion. Nat. Commun. 8, 15926.
Jin, S., Plikus, M.V., Nie, Q., 2025. CellChat for systematic analysis of cell-cell communication from single-cell transcriptomics. Nat. Protoc. 20 (1), 180–219.
Joo, Y., Kim, H., Lee, S., Lee, S., 2019. Neuronal growth regulator 1-deficient mice show increased adiposity and decreased muscle mass. Int. J. Obes. 43 (9), 1769–1782.
Kanehisa, M., Goto, S., 2000. KEGG: kyoto encyclopedia of genes and genomes. Nucleic Acids. Res. 28 (1), 27–30.
Kang, X., Yang, M.Y., Shi, Y.X., Xie, M.M., Zhu, M., Zheng, X.L., Zhang, C.K., Ge, Z.L., Bian, X.T., Lv, J.T., Wang, Y.J., Zhou, B.H., Tang, K.L., 2018. Interleukin-15 facilitates muscle regeneration through modulation of fibro/adipogenic progenitors. Cell Commun. Signal. 16 (1), 42.
Kesharwani, D., Brown, A.C., 2024. Navigating the adipocyte precursor niche: cell-cell interactions, regulatory mechanisms and implications for adipose tissue homeostasis. J. Cell Signal. 5 (2), 65–86.
La Manno, G., Soldatov, R., Zeisel, A., Braun, E., Hochgerner, H., Petukhov, V., Lidschreiber, K., Kastriti, M.E., Lönnerberg, P., Furlan, A., Fan, J., Borm, L.E., Liu, Z., van Bruggen, D., Guo, J., He, X., Barker, R., Sundström, E., Castelo-Branco, G., Cramer, P., Adameyko, L., Linnarsson, S., Kharchenko, P.V., 2018. RNA velocity of single cells. Nature 560 (7719), 494–498.
Li, D., Zhang, K., Pan, Z., Yu, M., Lu, Y., Wang, G., Wu, J., Zhang, J., Zhang, K., Du, W., 2020b. Antibiotics promote abdominal fat accumulation in broilers. Anim. Sci. J. 91 (1), e13326.
Livak, K.J., Schmittgen, T.D., 2001. Analysis of relative gene expression data using real-time quantitative PCR and the 2(-Delta Delta C(T)) method. Methods 25 (4), 402–408.
Li, X., Fu, X., Yang, G., Du, M., 2020a. Review: enhancing intramuscular fat development via targeting fibro-adipogenic progenitor cells in meat animals. Animal 14 (2), 312–321.
Li, Y., Yao, L., Lu, J., 2023. IL-35 inhibits adipogenesis via pparγ-wnt/β-catenin signaling pathway by targeting Axin2. Int. Immunopharmacol. 122, 110615.
Li, Y., Huang, X., Yang, G., Xu, K., Yin, Y., Brecchia, G., Yin, J., 2022. CD36 favours fat sensing and transport to govern lipid metabolism. Prog. Lipid Res. 88, 101193.
Macotela, Y., Emanuelli, B., Mori, M.A., Gesta, S., Schulz, T.J., Tseng, Y.H., Kahn, C.R., 2012. Intrinsic differences in adipocyte precursor cells from different white fat depots. Diabetes 61 (7), 1691–1699.
Malgwi, I.H., Halas, V., Grünvald, P., Schiavon, S., Jócsák, I., 2022. Genes related to fat metabolism in pigs and intramuscular fat content of pork: a focus on nutrigenetics and nutrigenomics. Animals 12 (2), 150.
Nahmgoong, H., Jeon, Y.G., Park, E.S., Choi, Y.H., Han, S.M., Park, J., Ji, Y., Sohn, J.H., Han, J.S., Kim, Y.Y., Hwang, I., Lee, Y.K., Huh, J.Y., Choe, S.S., Oh, T.J., Choi, S.H., Kim, J.K., Kim, J.B., 2022. Distinct properties of adipose stem cell subpopulations determine fat depot-specific characteristics. Cell Metab. 34 (3), e6.
Pyrina, I., Chung, K.J., Michailidou, Z., Koutsilieris, M., Chavakis, T., Chatzigeorgiou, A., 2020. Fate of adipose progenitor cells in obesity-related chronic inflammation. Front. Cell Dev. Biol. 8, 644.
Rivera-Gonzalez, G.C., Butka, E.G., Gonzalez, C.E., Mintz, R.L., Kleb, S.S., Josephson, V., Kong, W., Jindal, K., Kamimoto, K., Shook, B.A., Rodeheffer, M.S., Morris, S.A., 2025. Comparative single-cell lineage tracing identifies distinct adipocyte precursor dynamics in skin and inguinal fat. Cell Stem Cell 32 (8), e8.
Roca-Rivada, A., Castelao, C., Senin, L.L., Landrove, M.O., Baltar, J., Belén Crujeiras, A., Seoane, L.M., Casanueva, F.F., Pardo, M., 2013. FNDC5/irisin is not only a myokine but also an adipokine. PLoS. One 8 (4), e60563.
Schreiber, I., Dörpholz, G., Ott, C.E., Kragesteen, B., Schanze, N., Lee, C.T., Köhrle, J., Mundlos, S., Ruschke, K., Knaus, P., 2017. BMPs as new insulin sensitizers: enhanced glucose uptake in mature 3T3-L1 adipocytes via pparγ and GLUT4 upregulation. Sci. Rep. 7 (1), 17192.
Sebo, Z.L., Rodeheffer, M.S., 2019. Assembling the adipose organ: adipocyte lineage segregation and adipogenesis in vivo. Development 146 (7), dev172098.
Smas, C.M., Sul, H.S., 1993. Pref-1, a protein containing EGF-like repeats, inhibits adipocyte differentiation. Cell 73 (4), 725–734.
Suchanecka, M., Grzelak, J., Farzaneh, M., Azizidoost, S., Dari, M.A.G., Józkowiak, M., Data, K., Domagała, D., Niebora, J., Kotrych, K., Czerny, B., Kamiński, A., Torlińska-Walkowiak, N., Bieniek, A., Szepietowski, J., Piotrowska-Kempisty, H., Dzięgiel, P., Mozdziak, P., Kempisty, B., 2025. Adipose derived stem cells - sources, differentiation capacity and a new target for reconstructive and regenerative medicine. Biomed. PharmacOther 186, 118036.
Sun, Z., Liu, Z., Xi, J., Liu, Y., Zheng, Z., Li, N., Li, Z., Liang, S., Li, Q., Zhang, H., Yan, J., Sun, C., Mu, S., 2023. Effects of myonectin on porcine intramuscular adipocyte differentiation and exogenous free fatty acid utilization. Anim. Biotechnol. 34 (8), 3757–3764.
Sul, H.S., 2009. Minireview: pref-1: role in adipogenesis and mesenchymal cell fate. Mol. Endocrinol. 23 (11), 1717–1725.

Trapnell, C., Cacchiarelli, D., Grimsby, J., Pokharel, P., Li, S., Morse, M., Lennon, N.J., Livak, K.J., Mikkelsen, T.S., Rinn, J.L., 2014. The dynamics and regulators of cell fate decisions are revealed by pseudotemporal ordering of single cells. Nat. Biotechnol. 32 (4), 381–386.

Wu, T., Hu, E., Xu, S., Chen, M., Guo, P., Dai, Z., Feng, T., Zhou, L., Tang, W., Zhan, L., Fu, X., Liu, S., Bo, X., Yu, G., 2021. clusterProfiler 4.0: a universal enrichment tool for interpreting omics data. Innovation 2 (3), 100141.

Xu, D., Zhuang, S., Chen, H., Jiang, M., Jiang, P., Wang, Q., Wang, X., Chen, R., Tang, H., Tang, L., 2024. IL-33 regulates adipogenesis via wnt/β-catenin/PPAR-γ signaling pathway in preadipocytes. J. Transl. Med. 22 (1), 363.

Yang, C., Wang, Z., Song, Q., Dong, B., Bi, Y., Bai, H., Jiang, Y., Chang, G., Chen, G., 2022. Transcriptome sequencing to identify important genes and lncRNAs regulating abdominal fat deposition in duck. Animals 12 (10), 1256.

Yang Loureiro, Z., Joyce, S., DeSouza, T., Solivan-Rivera, J., Desai, A., Skritakis, P., Yang, Q., Ziegler, R., Zhong, D., Nguyen, T.T., MacDougald, O.A., Corvera, S., 2023. Wnt signaling preserves progenitor cell multipotency during adipose tissue development. Nat. Metab. 5 (6), 1014–1028.

Zhang, L., Uezumi, A., Kaji, T., Tsujikawa, K., Andersen, D.C., Jensen, C.H., Fukada, S.I., 2019. Expression and functional analyses of Dlk1 in muscle stem cells and mesenchymal progenitors during muscle regeneration. Int. J. Mol. Sci. 20 (13), 3269.

Zhang, X.Y., Wu, M.Q., Wang, S.Z., Zhang, H., Du, Z.Q., Li, Y.M., Cao, Z.P., Luan, P., Leng, L., Li, H., 2018. Genetic selection on abdominal fat content alters the reproductive performance of broilers. Animal 12 (6), 1232–1241.